



This is a repository copy of *Control of polarization and mode mapping of small volume high Q micropillars* .

White Rose Research Online URL for this paper:
<http://eprints.whiterose.ac.uk/3413/>

Article:

Daraei, A., Sanvitto, D., Timpson, J.A. et al. (9 more authors) (2007) Control of polarization and mode mapping of small volume high Q micropillars. *Journal of Applied Physics*, 102 (043105). ISSN 0021-8979

<https://doi.org/10.1063/1.2769803>

Reuse

Unless indicated otherwise, fulltext items are protected by copyright with all rights reserved. The copyright exception in section 29 of the Copyright, Designs and Patents Act 1988 allows the making of a single copy solely for the purpose of non-commercial research or private study within the limits of fair dealing. The publisher or other rights-holder may allow further reproduction and re-use of this version - refer to the White Rose Research Online record for this item. Where records identify the publisher as the copyright holder, users can verify any specific terms of use on the publisher's website.

Takedown

If you consider content in White Rose Research Online to be in breach of UK law, please notify us by emailing eprints@whiterose.ac.uk including the URL of the record and the reason for the withdrawal request.



eprints@whiterose.ac.uk
<https://eprints.whiterose.ac.uk/>

promoting access to White Rose research papers



Universities of Leeds, Sheffield and York
<http://eprints.whiterose.ac.uk/>

This is an author produced version of a paper published in **Journal of Applied Physics**.

White Rose Research Online URL for this paper:
<http://eprints.whiterose.ac.uk/3413/>

Published paper

Daraei, A., Sanvitto, D., Timpson, J.A., Fox, A.M., Whittaker, D.M., Skolnick, M.S., Guimaraes, P.S.S., Vinck, H., Tahraoui, A., Fry, P.W., Liew, S.L. and Hopkinson, M. (2007) *Control of polarization and mode mapping of small volume high Q micropillars*, Journal of Applied Physics, Volume 102 (4).

Control of polarization and mode mapping of small volume high Q micropillars

A. Daraei,* D. Sanvitto, J. A. Timpson, A. M. Fox, D. M. Whittaker, and M. S. Skolnick

*Department of Physics and Astronomy,
University of Sheffield, Sheffield S3 7RH, UK*

P. S. S. Guimarães

*Departamento de Física, Universidade Federal de Minas Gerais,
30123-970, Belo Horizonte, Minas Gerais, Brazil*

H. Vinck

Instituto de Física, Universidad de Antioquia, AA 1226 Medellín, Colombia

A. Tahraoui, P. W. Fry, S. L. Liew, and M. Hopkinson

*Department of Electronic and Electrical Engineering,
University of Sheffield, Sheffield S1 3JD, UK*

(Dated: May 29, 2007)

Abstract

We show that the polarization of the emission of a single quantum dot embedded within a microcavity pillar of elliptical cross section can be completely controlled and even switched between two orthogonal linear polarizations by changing the coupling of the dot emission with the polarized photonic modes. We also measure the spatial profile of the emission of a series of pillars with different ellipticities and show that the results can be well described by simple theoretical modeling of the modes of an infinite length elliptical cylinder.

I. INTRODUCTION

A robust and reliable source of anti-bunched photons, that is, an on-demand single photon source, is essential for the implementation of quantum information applications like quantum computation and quantum cryptography. Self assembled semiconductor quantum dots (QDs) have been fully confirmed as an effective single photon source.^{1,2} Their ease of fabrication and their compatibility with present day devices and with advanced processing techniques makes them very attractive for these applications. However, in order to achieve an efficient source, the quantum dots have to be embedded in a small volume (V), high quality factor (Q) cavity, to take advantage of the Purcell effect to enhance the spontaneous emission and to improve collection efficiency.^{3,4} Several approaches are being considered for the implementation of the photonic cavity.⁵ Defects in a photonic crystal, whispering gallery microcavities of different geometries and micropillar cavities are the three concepts most intensely explored. The third approach offers as main advantages an expected good collection efficiency⁶ and relatively easy integration with other opto-electronic devices. By altering the shape of the micropillars, the photonic mode structure can be controlled to some extent. It has already been demonstrated that in pillars with an elliptical cross section the polarization degeneracy of the modes is lifted.⁷⁻⁹ The achievement of a Purcell enhancement for just one polarized state of the quantum dots is a desirable feature since polarization degeneracy is a potential source of noise. In addition, we have also recently demonstrated¹⁰ that in elliptical micropillars the photonic mode polarized parallel to the major axis of the ellipse have a Q/V ratio significantly greater than can be achieved in a circular pillar of similar volume. Therefore, these structures are very interesting for all applications that require the maximization of the Purcell effect, where one desires a large Q/V , and for the study of strong coupling effects, which needs structures with a large Q/\sqrt{V} ratio.⁴

In this paper we show that the polarization of the quantum dot emission in microcavity pillars with elliptical cross section can be completely controlled. We demonstrate that the linearly polarized emission of a single dot within the elliptical microcavity pillar can be changed between two orthogonal directions by coupling the excitonic dot emission alternately to the polarized lowest energy modes of the cavity. We also measure the spatial profile of the emission for the photonic modes of a series of microcavity micropillars with increasing degree of ellipticity. We show that the spatial distribution of light emission in these structures is

well explained by a theoretical model that considers the photonic modes of an infinite length elliptical cylinder with quantized modes in the waveguide direction. In this way, we are able to identify each mode of our pillars and understand the order in energy in which they occur.

II. EXPERIMENTAL

The samples studied in this work were fabricated from planar microcavity material which was grown by molecular beam epitaxy. *In situ* optical reflectivity monitoring was employed during growth to control the thicknesses of the deposited layers. The as-grown planar microcavities have $Q \approx 30000$.¹¹ They consist of a one wavelength thick GaAs cavity surrounded by lower and upper distributed Bragg reflectors (DBR) containing 27 and 20 GaAs/Al_{0.8}Ga_{0.2}As layer repeats, respectively. A layer of InAs dots with density $\lesssim 10^{10} \text{ cm}^{-2}$ was embedded in the center of the GaAs cavity. Figure 1 (a) is a transmission electron microscope image of the cavity region. To fabricate the micropillars, first a 600 nm layer of SiO₂ was deposited, followed by spin coating of 300 nm of polymethyl methacrylate (PMMA). Then, electron beam lithography was used to pattern the PMMA layer. A 100 nm thick layer of aluminum was evaporated and the pattern transferred by lift-off to leave metal discs which serve as a mask to etch the SiO₂ by CHF₃-based reactive ion etching. Finally, after chemically removing the metal, SiCl₄/Cl₂-based inductively coupled plasma (ICP) reactive ion etching was used to form the pillars. The SiO₂ layer facilitates the etching of high aspect ratio pillars and inhibits sidewall degradation which would otherwise occur during the removal of the aluminum mask.

The fabricated structures include micropillars of circular cross section with different diameters, and of elliptical cross section with different ellipticities and sizes. Figure 1(b) shows a scanning electron microscope image of an elliptical cross section pillar. The sidewall smoothness seen in this pillar is typical for all the sizes and shapes fabricated. Pillars with sizes $\gtrsim 1 \mu\text{m}$ also show good verticality for aspect ratios as high as 8:1.

The optical studies reported here were performed in a standard micro-photoluminescence setup, with spectral resolution better than 0.04 nm, for temperatures between 4 K and 60 K. Excitation was provided by the 632.8 nm line of a He-Ne laser, focused with a 50 X magnification microscope objective to a spot of $\lesssim 2 \mu\text{m}$ diameter. The spectrally resolved spatial profiles of the emission were recorded using an imaging spectrometer and a charge

coupled device (CCD) camera. For all measurements, the sample is mounted inside a cold finger cryostat with a short window-to-sample distance. Care was taken that at all excitation powers heating of the sample by the laser was not significant.

III. CONTROL OF POLARIZATION OF A SINGLE QUANTUM DOT EMISSION

As reported before⁹ the microcavity pillars investigated here exhibit high quality factors Q , with values up to 13000 for a $1.5 \mu\text{m}$ diameter circular pillar. In pillars with an elliptical cross section, the polarization degeneracy of the photonic modes is lifted into two orthogonally linearly polarized modes, with polarizations parallel (X , lower energy mode) and perpendicular (Y , higher energy mode) to the long axis of the pillar. Figure 2 shows the polarization splitting of the fundamental mode in the emission spectra of a series of elliptical pillars with different ellipticities. As expected,⁷ the splitting increases with ellipticity. We note also that there is a pronounced difference in the Q -values of the two polarized modes. As explained elsewhere,¹⁰ this difference is due to the polarization sensitivity of the reflectivity of the Bragg mirrors.

The spectra shown in Fig. 2 are obtained under high power excitation. In this condition, the emission lines from single dots within the pillars are saturated and only the photonic modes of the pillars are seen. Under low power excitation, emission from individual dots is resolved. When spectrally separated from the photonic modes, the dot photoluminescence lines are normally unpolarized, since the dots typically have nearly degenerate orthogonally polarized exciton transitions. In some dots a small polarization splitting is resolvable.¹² By contrast, the emission of a quantum dot in resonance with one of the polarized photonic modes of an elliptical pillar is normally strongly polarized,⁹ showing the same polarization as the mode.

Figure 3 shows emission spectra at 7 K with low excitation power for two orthogonal polarizations for an elliptical pillar with a $2 \mu\text{m}$ major axis and a $1.5 \mu\text{m}$ minor axis. Although the excitation power is low, the polarization split fundamental photonic mode can still be seen clearly. The polarization splitting, about 0.3 nm, is relatively small due to the low degree of ellipticity of this pillar but since the Q values are high, around 10000, the strongly polarized lines are well resolved. An excitonic emission from a quantum dot is seen at a energy just above the fundamental photonic mode. Note that the emission of this

out-of-resonance dot is not polarized.

With an increase in temperature, the dot excitonic emission shifts to lower energy due, mainly, to the change in the energy bandgap of the material. The photonic modes also shift to lower energy with temperature, but at a much slower rate, largely due to the change in the refractive indexes. Hence, the emission of a quantum dot may be scanned through resonance with the photonic modes by temperature variation (see, e.g., Daraei et al.⁹). Figure 4 shows such a temperature scan, for the same sample shown in Fig. 3. The excitonic dot emission seen at an energy just above resonance with the Y polarized mode is gradually swept across the two polarized modes of the elliptical micropillar. It is evident in the spectra that as the dot comes into resonance first with the Y polarized mode, then with the lower energy X polarized mode its emission in the corresponding polarization is enhanced while the emission in the opposite polarization is suppressed. This change in the polarization of the single quantum dot emission as it is tuned across the individual polarized photonic modes is more clearly seen in Figure 5 which shows the degree of polarization of the single dot emission as a function of the energy at which the emission occurs for each temperature. The degree of polarization is defined by $\rho = (I_X - I_Y)/(I_X + I_Y)$, where I_X and I_Y are, respectively, the intensities for polarizations parallel and perpendicular to the major axis of the elliptical cross section. Photoluminescence spectra at high excitation power are also shown in the figure to indicate the position and linewidth of the photonic modes. The polarization of the single dot changes from zero to more than 70% Y polarization, back to zero, then to above 95% X polarization and back to zero polarization again, as the excitonic emission is tuned across the photonic modes. This shows that the polarization of the emission from a single quantum dot can be fully controlled by tuning its emission through the modes of the elliptical pillar.

IV. SPECTRALLY RESOLVED TWO DIMENSIONAL PHOTONIC MODE MAPPING

Further insight into the coupling of the emission of the dots to the photonic modes and also into the structure of the modes themselves can be obtained by measuring the spatial distribution of the optical emission out of the microcavity pillar. Figure 6(a) shows one-dimensional (1D) cross sectional images of the first three modes for an elliptical pillar with

5 μm - 1 μm major axis - minor axis, such as the one shown in Fig. 1(b), in Y polarization at high excitation power. At each energy we plot a one-dimensional cross section through the image of the emission. The spatial profile of the first three photonic modes along the major axis of the elliptical cross section of the pillar shows clearly the variation of spatial distribution with mode number. Figure 6(b) shows the corresponding photoluminescence spectra for the two polarizations, at high excitation power, which displays the photonic modes, and at low power, in which the emission from single quantum dots is resolved. Note that some dots, such as the one indicated by the third arrow from the left in Fig. 6(b), do not couple well to the photonic modes as far as the degree of polarization is concerned. This is probably due to these dots being located at or near a node of the mode to which they are spectrally tuned. Figure 6(c) is a 1D spatial profile obtained at low power in Y polarization, showing the spatial distribution of the emission of single quantum dots, for this polarization. It is striking that for all dots the excitonic emission shows the same spatial pattern of emission of the mode with which it is on, or nearly on, resonance. Although the spatial distribution is the same, the images of the modes, Fig. 6(a), are spectrally broader than the images of the individual dots shown in Fig. 6(c).

Two dimensional (2D) spectrally resolved cross sectional maps of the light emission can be obtained by measuring a sequence of 1D spatial profiles. A 2D cross sectional map is constructed for each emission energy by combining 1D profiles such as the ones shown in Fig. 6, each one of them obtained at a different imaging position along the direction perpendicular to the one at which the 1D profile is measured. The bottom part of Figure 7 shows four 2D maps for a 5 μm diameter circular pillar, at the wavelengths corresponding to the four lowest energy photonic modes. Apart from small deviations, all mode maps measured in circular micropillars show the expected circular symmetry. The top part of Fig. 7 shows calculations of the magnitude of the normal component of the Poynting vector for the 5 μm diameter pillar. The calculations are performed for an infinite circular cylinder, using a plane wave expansion for the transverse profile of the mode. The effects of vertical confinement are modeled by considering solutions with a finite wavevector, k_{\parallel} , along the axis of the cylinder. This is chosen to give the correct mode energy for the planar structure. The good agreement between the experimental mode images and their calculated counterparts allows us to identify each mode up to the 7th order. At the same time we show that the lateral confinement of the micropillar optical modes can be relatively easily modeled by

using waveguide theories. However, the vertical confinement and lateral leakage are strongly dependent on the effects of the top and bottom DBR mirrors and can only be studied with more realistic three-dimensional models such as the finite difference time domain (FDTD) technique, albeit at the expense of much longer calculation times.¹⁰

Figure 8 shows 2D spectrally resolved maps for the photoluminescence emission of a series of elliptical micropillars with increasing degree of ellipticity. The major axis of the elliptical cross section of all pillars is $5 \mu\text{m}$ and the minor axis is $4 \mu\text{m}$ in Fig. 8(a), $3 \mu\text{m}$ in Fig. 8(b), $2 \mu\text{m}$ in Fig. 8(c) and $1 \mu\text{m}$ in Fig. 8(d). For each case, the bottom row shows the measured 2D spatial distribution of the emission from the top of the pillar for Y polarization and the top row displays the results of a calculation of the magnitude of the normal component of the Poynting vector at the corresponding wavelengths and polarization. Similar to the circular pillars, the calculations are for infinite cylinders of elliptical cross section, with the longitudinal wave vector chosen to represent the confinement along the growth direction. Their reliability is demonstrated by the excellent agreement with the experimentally determined optical mode profiles, as seen in Fig. 8. It is interesting to note that as the degree of ellipticity increases, from Fig. 8(a) to Fig. 8(d), photonic modes that have a spatial distribution more akin to the increasingly elliptical shape change order with the modes that conform less to the elliptical cross section. For instance, the third and fourth modes of the $5 \mu\text{m} - 3 \mu\text{m}$ pillar have shapes that correspond respectively to the fourth and third modes of the $5 \mu\text{m} - 2 \mu\text{m}$ pillar. In the same way, modes 5 and 6 of the same pillars also swap their energy position as we go from the $5 \mu\text{m} - 3 \mu\text{m}$ to the $5 \mu\text{m} - 2 \mu\text{m}$ pillar. The change in order of the modes can be understood in terms of the relative strengths of the confinement in the two directions. In the $5 \mu\text{m} - 1 \mu\text{m}$ structures, Fig. 8(d), the confinement energy is very large along the minor (Y) axis, so a sequence of modes with increasing number of nodes along the major (X) axis is seen. In the wider pillars, the minor axis confinement is weaker, so the higher order modes in that direction appear earlier in the sequence, as shown in Figs 8(c), 8(b) and 8(a).

V. SUMMARY AND CONCLUSIONS

We have shown that it is possible to control completely the linear polarization of the emission from single quantum dots. This is achieved by embedding the quantum dots inside

a microcavity pillar with elliptical cross section and using temperature variation to tune the quantum dot emission in and out of resonance alternately with the polarization split photonic modes of the elliptical micropillar. Taken together with the ease of fabrication of these structures, this confirms microcavity pillars with an asymmetric cross section as very attractive devices for polarized single photon sources.

In addition, we have measured the spatial distribution of the light emission for a series of elliptical cross section microcavity micropillars, showing the different photonic mode emission patterns and how they change with the variation in ellipticity. The experimental results are in good agreement with a calculation based on the finite wave vector modes of a homogeneous infinite length pillar with the longitudinal wave vector chosen to represent the confinement along the growth direction. The spatial profiles of the light emitted by single quantum dots confirms that the excitonic emission of a dot in resonance with a photonic mode is funneled into that particular mode.

Acknowledgments

We acknowledge support from EPSRC grant number GR/S76076 and the QIPIRC. AD acknowledges sponsorship from MSRT, Iran. PSSG acknowledges support from FAPEMIG and CNPq, Brazil.

REFERENCES

- * on leave of absence from University of Sistan and Baluchestan, Zahedan, Iran
- ¹ E. Moreau, I. Robert, J. M. Gerard, I. Abram, L. Manin, and V. Thierry-Mieg, *Applied Physics Letters* **79**, 2865 (2001).
- ² R. M. Thompson, R. M. Stevenson, A. J. Shields, I. Farrer, C. J. Lobo, D. A. Ritchie, M. L. Leadbeater, and M. Pepper, *Physical Review B* **64**, 201302 (2001).
- ³ J. M. Gerard, B. Sermage, B. Gayral, B. Legrand, E. Costard, and V. Thierry-Mieg, *Physical Review Letters* **81**, 1110 (1998).
- ⁴ J. M. Gerard and B. Gayral, *Physica E* **9**, 131 (2001).
- ⁵ K. J. Vahala, *Nature* **424**, 839 (2003).
- ⁶ W. L. Barnes, G. Bjork, J. M. Gerard, P. Jonsson, J. A. E. Wasey, P. T. Worthing, and V. Zwiller, *The European Physical Journal D* **18**, 197 (2002).
- ⁷ B. Gayral, J. M. Gérard, B. Legrand, E. Costard, and V. Thierry-Mieg, *Applied Physics Letters* **72**, 1421 (1998).
- ⁸ D. C. Unitt, A. J. Bennett, P. Atkinson, D. A. Ritchie, and A. Shields, *Physical Review B* **72**, 033318 (2005).
- ⁹ A. Daraei, A. Tahraoui, D. Sanvitto, J. A. Timpson, P. W. Fry, M. Hopkinson, P. S. S. Guimarães, H. Vinck, D. M. Whittaker, M. S. Skolnick, et al., *Applied Physics Letters* **88**, 051113 (2006).
- ¹⁰ D. M. Whittaker, P. S. S. Guimarães, D. Sanvitto, H. Vinck, S. Lam, A. Daraei, J. A. Timpson, A. M. Fox, M. S. Skolnick, Y.-L. D. Ho, et al., *Applied Physics Letters* **90**, 161105 (2007).
- ¹¹ D. Sanvitto, A. Daraei, A. Tahraoui, M. Hopkinson, P. W. Fry, D. M. Whittaker, and M. S. Skolnick, *Applied Physics Letters* **86**, 191109 (2005).
- ¹² M. Bayer, A. Kuther, A. Forchel, A. Gorbunov, V. B. Timofeev, F. Schäfer, J. P. Reithmaier, T. L. Reinecke, and S. N. Walck, *Physical Review Letters* **82**, 1748 (1999).

LIST OF FIGURE CAPTIONS

FIGURE 1 - (a) Transmission electron microscope image of the cavity region of the as-grown microcavity sample. (b) Scanning electron micrograph of an elliptical pillar in which the major and minor axes of the elliptical cross section are $5\ \mu\text{m}$ and $1\ \mu\text{m}$ long, respectively.

FIGURE 2 - (Color online) Polarization resolved photoluminescence spectra under high excitation power ($\approx 300\ \mu\text{W}$) for a series of microcavity pillars with elliptical cross section, showing the photonic modes of lowest energy for each pillar. The major axis of the ellipses is $2.0\ \mu\text{m}$ in all cases while the minor axis is (a) $0.6\ \mu\text{m}$, (b) $0.8\ \mu\text{m}$, (c) $1.0\ \mu\text{m}$, (d) $1.5\ \mu\text{m}$. The spectra shown are linearly polarized either along the major axis (X polarization) or the minor axis (Y polarization) of the ellipses.

FIGURE 3 - (color online) Photoluminescence at low power excitation ($\approx 1.6\ \mu\text{W}$) from an elliptical pillar with $2\ \mu\text{m}$ long major axis and $1.5\ \mu\text{m}$ long minor axis measured at $7\ \text{K}$ at two orthogonal polarizations, X and Y . The two broader features are the polarization split lines of the fundamental photonic mode. The unpolarized emission at higher energy comes from exciton recombination.

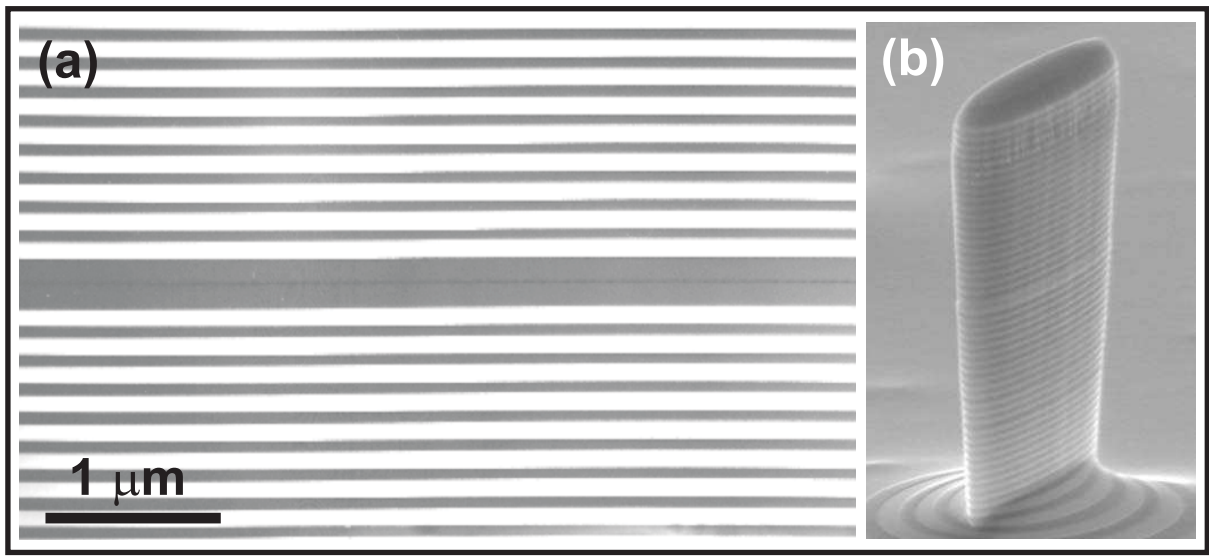
FIGURE 4 - (color online) Temperature scanning of a single quantum dot emission across the polarization split fundamental photonic mode of a $2\ \mu\text{m} - 1.5\ \mu\text{m}$ elliptical microcavity pillar. Since for this pillar the polarization splitting is small but the modes are well resolved, a single dot can be scanned sequentially through resonance with both polarized modes by a relatively small temperature change. Spectra are shown for temperatures between $7\ \text{K}$ (top) up to $41\ \text{K}$ (bottom) for two orthogonal polarizations, parallel to the major axis (X polarization) and to the minor axis (Y polarization) of the ellipse. As the temperature increases the dot emission is tuned into resonance first with the Y polarized mode, than with the lower energy X polarized mode. As the dot emission comes into resonance with each polarized mode, an enhancement is observed for the corresponding polarization while the emission at the opposite polarization is strongly reduced.

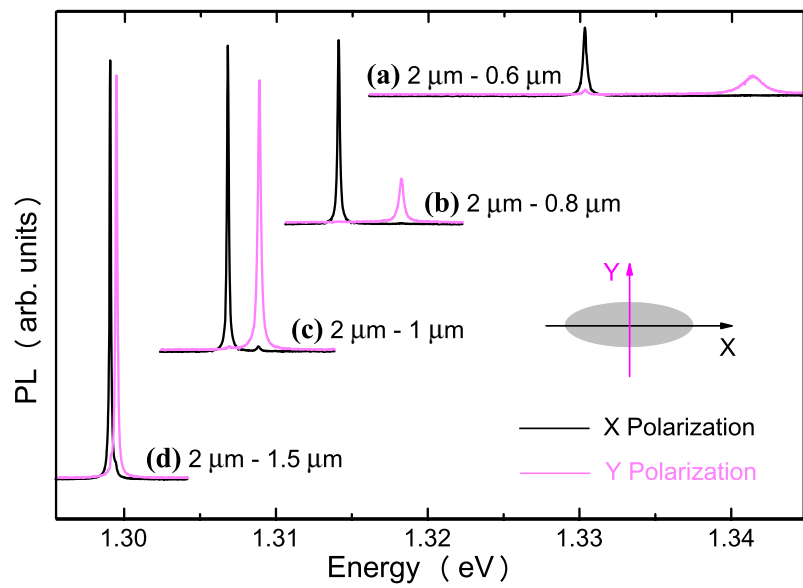
FIGURE 5 - (Color online) Variation of the degree of polarization (squares) of the quantum dot emission seen in Fig. 3 as the temperature is changed from $7\ \text{K}$ to $44\ \text{K}$. The degree of polarization is shown as a function of the energy at which the emission of the dot occurs for each temperature. High power photoluminescence spectra at X (black line) and Y (gray line) polarizations are also displayed to show the positions and linewidths of the polarized photonic modes of the elliptical pillar at the temperatures at which the resonances occur.

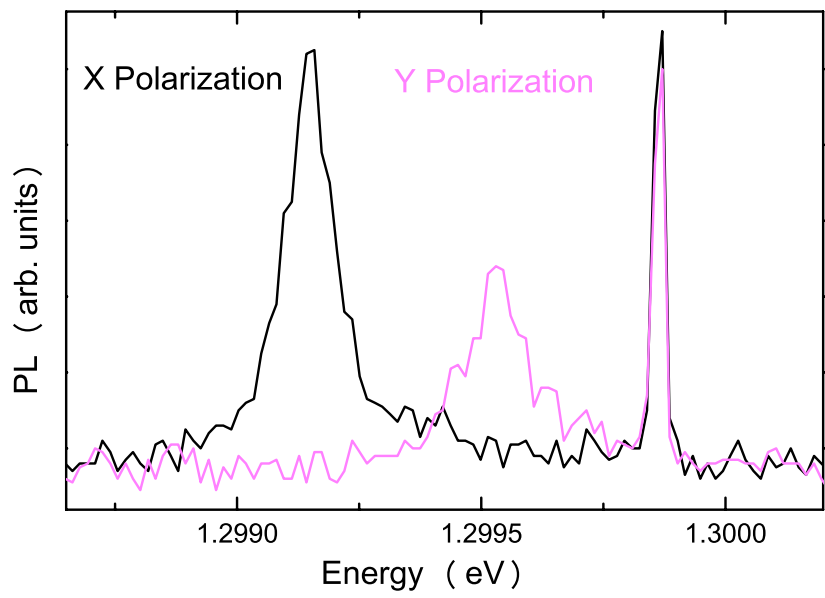
FIGURE 6 - (Color online) (a) Spatially resolved photoluminescence taken along the major axis of an elliptical pillar with $5\ \mu\text{m}$ - $1\ \mu\text{m}$, major axis - minor axis, in Y polarization at high excitation power. The spatial distribution of the emission of the first three photonic modes can be seen. (b) High and low excitation power photoluminescence spectra at X and Y polarizations for the same pillar. The high power spectra show the photonic modes of this pillar while the low power spectra allow the visualization of the emission of single quantum dots. Five quantum dots which emit strongly in Y polarization are indicated by the arrows. (c) Spatially resolved photoluminescence at Y polarization, at low excitation power, for the same pillar. The spatial distribution of the emission from individual quantum dots is resolved.

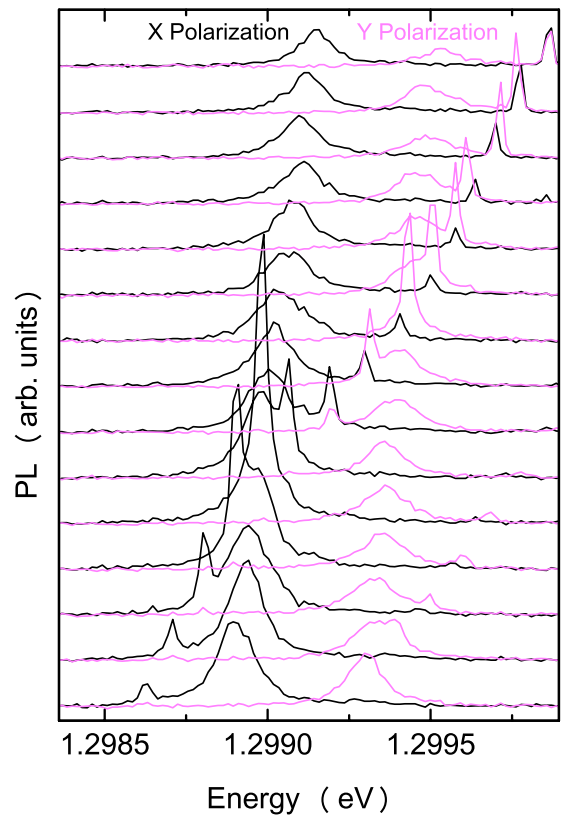
FIGURE 7 - (Color online) Two dimensional spatial distribution of the photoluminescence emission from the top of a $5\ \mu\text{m}$ diameter circular microcavity pillar. Each image in the bottom row is the measured 2D spectrally resolved mode map at the energy of a photonic mode of this pillar. The first four modes are shown. The top row shows calculations of the magnitude of the normal component of the Poynting vector at the corresponding energies, as explained in the text.

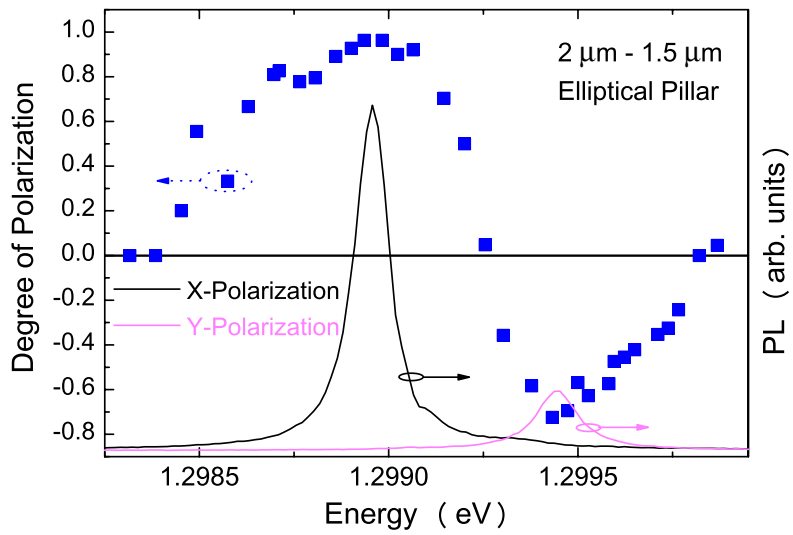
FIGURE 8 - (Color online) Two dimensional spatial distribution of the photoluminescence emission from the top of a series of microcavity pillars of elliptical cross sections, all with $5\ \mu\text{m}$ long major axis and minor axis of length $4\ \mu\text{m}$ (a), $3\ \mu\text{m}$ (b), $2\ \mu\text{m}$ (c) and $1\ \mu\text{m}$ (d). Each image in a row is obtained at the energy of a photonic mode of that pillar, with mode order increasing from left to right. For each pillar, the bottom row is the measured 2D spectrally resolved mode map and the top row is a calculation of the magnitude of the normal component of the Poynting vector at the corresponding photonic mode energies.

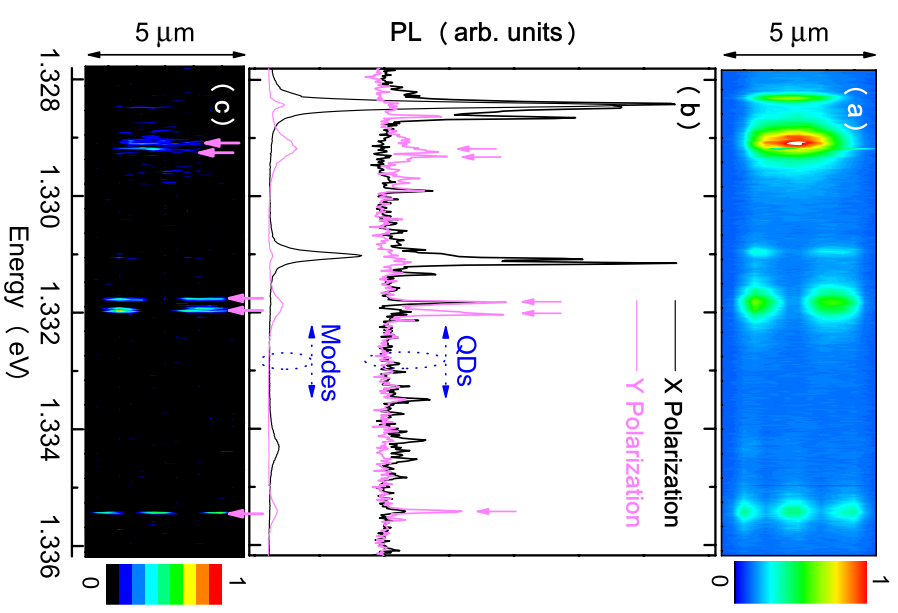


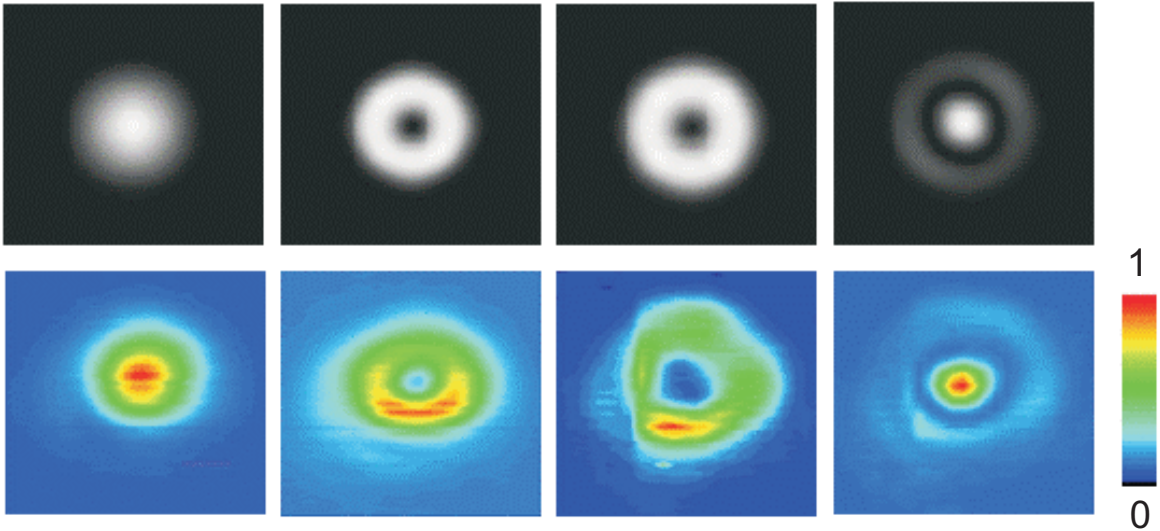












Increasing Energy



